APS physics

CHORUS

This is the accepted manuscript made available via CHORUS. The article has been published as:

Response to a local quench of a system near the many-body localization transition

Canran Xu and Maxim G. Vavilov

Phys. Rev. B **95**, 085139 — Published 24 February 2017

DOI: 10.1103/PhysRevB.95.085139

Response to a local quench of a system near many body localization transition

Canran Xu and Maxim G. Vavilov
Department of Physics, University of Wisconsin-Madison, Wisconsin 53706, USA
(Dated: January 24, 2017)

We consider a one dimensional spin 1/2 chain with Heisenberg interaction in a disordered parallel magnetic field. This system is known to exhibit the many body localization (MBL) transition at critical strength of disorder. We analyze the response of the chain when additional perpendicular magnetic field is applied to an individual spin and propose a method for accurate determination of the mobility edge via local spin measurements. We further demonstrate that the exponential decrease of the spin response with the distance between perturbed spin and measured spin can be used to characterize the localization length in the MBL phase. We also studied effect of the quench on statistics of the entire energy spectrum. We demonstrate that the quench introduces level repulsion between energy states corresponding to different eigenvalues of the total spin in the delocalized regime, while level spacing is described by the Poisson statistics in the localized regime even at strong quench.

I. INTRODUCTION

Theoretical studies of localization in many body systems were originally focused on interacting electrons in disordered metals [1]. Even though the localization endures through high temperature limit [2], an experimental observation of localization is a challenging task due to electron-phonon interaction that effectively spoils many-particle states of the electron system in real metals [3]. The interest in observation of many-body localization (MBL) has shifted to artificial quantum systems well isolated from their environment such as ultra-cold atomic gases [4], trapped ions [5, 6] and superconducting circuits containing many interacting spins [7]. These systems have highly configurable Hamiltonians and their observables can be measured with high precision, which gives another advantage to artificial quantum systems over their solid state counterparts for studies of MBL.

Recent theoretical studies were focused on numerical and analytical studies of interacting one dimensional spins chains or one dimensional fermion systems [8–22]. Spin chains can be simulated numerically by exact diagonalization of corresponding Hamiltonians for relatively small number of quantum particles or by approximate methods with controllable accuracy. These studies have shown that spin systems containing more than ten spins and involving thousands of many-body eigenstates exhibit the MBL behavior in sufficiently strong disorder. The MBL phase can be characterized by the existence of infinite number of local integrals of motion [8–11, 20], the entanglement [12–17], as well as the spectral properties of eigenstates[2]. While these characteristics can be measured in principle, the corresponding experiments are extremely burdened as they require either a full quantum tomography or full energy spectroscopy.

In this paper we propose an alternative strategy to identify the localization in a disordered system of interacting spins. We analyze the response of a pure state of a Heisenberg spin chain in random magnetic field along z axis to a sudden application of a magnetic field (quench) perpendicular to z that acts on a single spin. We evaluate the inverse participation ratio (IPR) of an eigenstate of unperturbed Hamiltonian in the basis of the quenched Hamiltonian. The IPR is small in the delocalized, or ergodic, regime when the initial state overlaps with many eigenstates of the new Hamiltonian. In the localized regime, an application of a quench does not affect majority of eigenstates and the typical value of the IPR is about unity. Points at which the IPR starts increasing sharply form a curve in the energy *vs* disorder strength plane and define the mobility edges. We note that due to finite size of our system, the mobility edge cannot be defined rigorously and instead has to be treated as a crossover region. Recently, the authors of Ref. [18] argued that even in infinite system MBL and ergodic phases are separated by a crossover region.

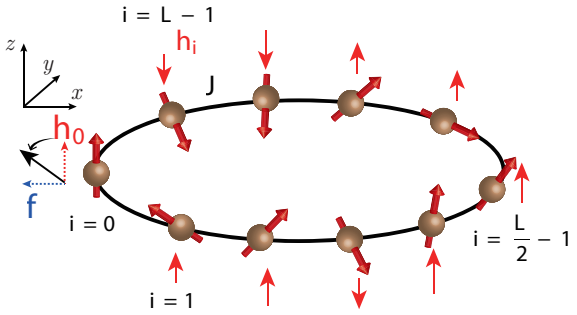

FIG. 1. Sketch of the one-dimensional spin-1/2 chain with periodic boundary condition. Along the chain, each spin is subject to a random onsite field h_i along z direction and the spins are coupled by nearest neighbor Heisenberg interactions with strength J. At time t_0 when the local quench is turned on, a transverse magnetic field f is applied to one of the spins, labeled by $i = 0$.

Since the IPR is not easily measurable in experiments, we also investigate correlations in single spin measurements before and after the quench. The covariance between these two measurements is small for delocalized states, but rapidly increases for localized states, as the quench only weakly affects configuration of far away spins. The mobility edge obtained from the covariance

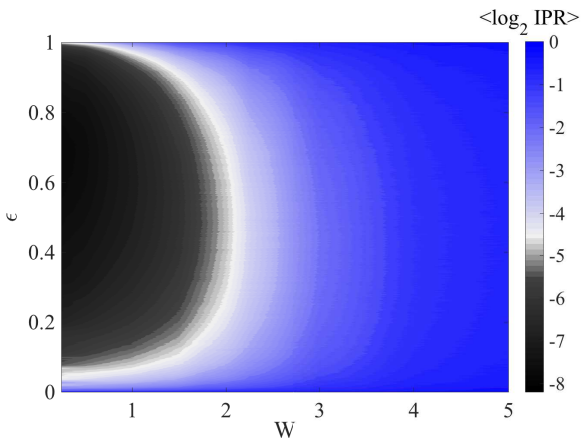

FIG. 2. (Color online) Average of $\log_2(IPR)$ over disorder realizations as functions of disorder strength W and energy density ϵ for a system of $L = 12$ and 2000 realizations. The quench strength is fixed at $f = J = 1$. Marked by gray area, the many body mobility edge encloses a region of delocalized states (black area) with IPR $\sim 2^{-L}$.

is consistent with the mobility edge obtained through the IPR, as well as through analysis of the entanglement entropy [23, 24]. Moreover, at strong disorder in the localization regime, the spin response to the quench decreases exponentially as a function of the distance of the monitored spin from the quenched spin. We utilize this exponential decay to evaluate the localization length as a function of disorder and demonstrate that the localization length exceeds the system size near the mobility edge.

We also analyze statistics of energy level spacing in response to a quench. The level spacing is determined by the matrix elements of the quench connecting two eigenstates of the original Hamiltonian. Such connectivity between states in the phase space acts as a probe of localization. As shown in Ref. [9], a local conserved quantity for MBL states are the local spins, dressed by their neighbors with strengths set by the many-body localization length ξ. If ξ is comparable to the lattice spacing, local spins are oblivious to each other, so that different spin configurations are weakly connected in the phase space. On the other hand, the local operators become extended once the localization length increases to the system size. Above arguments imply that the entire spectrum of a finite size system responds differently to quench in localized and ergodic regimes. The response to quench distinguishes the two phases and can be seen as a reminiscent of its non-local response that forms a rearrangement of local conserved quantities. In the thermodynamic limit, the two phases can be recognized if there is the orthogonality catastrophe due to small changes in the amplitude f. Unfortunately, this limit cannot be investigated numerically and calls for future work.

II. SYSTEM WITH A LOCAL QUENCH

To be specific, we consider a 1D Heisenberg spin chain of length L with random on-site field in the z direction with periodic boundary condition, described by the Hamiltonian, see Fig. 1:

$$H_0 = \sum_{i=0}^{L-1} h_i \sigma_z^{(i)} + J \sum_{i=0}^{L-1} \boldsymbol{\sigma}^{(i)} \cdot \boldsymbol{\sigma}^{(i+1)}, \tag{1}$$

where h_i on each site is a random variable distributed uniformly in the interval $[-W, W]$ and $\boldsymbol{\sigma}^{(i)}$ is the vector of Pauli matrices for spin at site i. Throughout the paper, we use J as a fundamental unit and set $J = 1$. We denote eigenstates of H_0 by $|\alpha_{S_z}\rangle$, where the total spin in z direction $S_z = (1/2)\sum_i \sigma_z^{(i)}$ is conserved for a system describe by Hamiltonian (1).

Previous numerical [9, 17, 25] and analytical [26] studies were focused on the subspace defined by energy states $|\alpha_0\rangle$ with $S_z = 0$, where the MBL phase develops at $W \gtrsim 3.4$. In this paper, we study the effect of the sudden quench

$$V = f\sigma_x^{(i=0)}, \tag{2}$$

applied to Hamiltonian (1) at site $i = 0$, see Fig. 1. The new Hamiltonian $\tilde{H} = H_0 + V$ breaks the conservation of S_z, and system dynamics occur in the full 2^L dimensional space with the basis defined by eigenvectors $|\tilde{\alpha}\rangle$ of $\tilde{H}$. We would like to emphasize that Ref. [9] considers a local quench that conserves total spin in z direction, while Ref. [17] analyzes the global quench uniformly applied to all spins. The response of the system to this quench is reminiscent to the quasiparticle spectral function that appears in transport problems in disordered electron systems with interactions. [27] In case when Hamiltonian (1) is applied to an actual spin or qubit chain, the quench, Eq. (2) can be introduced as a microwave field in the rotating frame approximation.

We consider a system that was originally prepared as a pure state $|\psi\rangle$ in the subspace of states with $S_z|\psi\rangle = 0$ and calculate its response over a long time after the onset of the quench:

$$\langle\bar{\mathcal{O}}\rangle = \lim_{T\to\infty} \frac{1}{T}\int_0^T \langle\hat{\mathcal{O}}(t)\rangle dt = \mathrm{Tr}\overline{\rho(t)\hat{\mathcal{O}}} = \mathrm{Tr}\{\rho_{\mathrm{DE}}^{|\psi\rangle}\hat{\mathcal{O}}\}, \tag{3}$$

where $\rho(t) = \exp(-i\tilde{H}t)\rho(0)\exp(i\tilde{H}t)$ is the density matrix and $\rho_{\mathrm{DE}}^{|\psi\rangle} = \overline{\rho(t)}$ is the time-averaged density matrix initialized in a pure state. Then, $\rho(0) = |\psi\rangle\langle\psi|$,

$$\rho_{\mathrm{DE}}^{|\psi\rangle} = \sum_{\tilde{\alpha}}^{2^L} \mathcal{P}_{\tilde{\alpha}} |\langle\tilde{\alpha}|\psi\rangle|^2, \quad \mathcal{P}_{\tilde{\alpha}} = |\tilde{\alpha}\rangle\langle\tilde{\alpha}| \tag{4}$$

and $\mathcal{P}_{\tilde{\alpha}}$ is the projection operator on new eigenstates $|\tilde{\alpha}\rangle$ of $\tilde{H}$. The off-diagonal elements of $\rho_{\mathrm{DE}}^{|\psi\rangle}$ vanish after time averaging and matrices $\rho_{\mathrm{DE}}^{|\psi\rangle}$ belong to a diagonal ensemble [28]. In particular, we consider initial

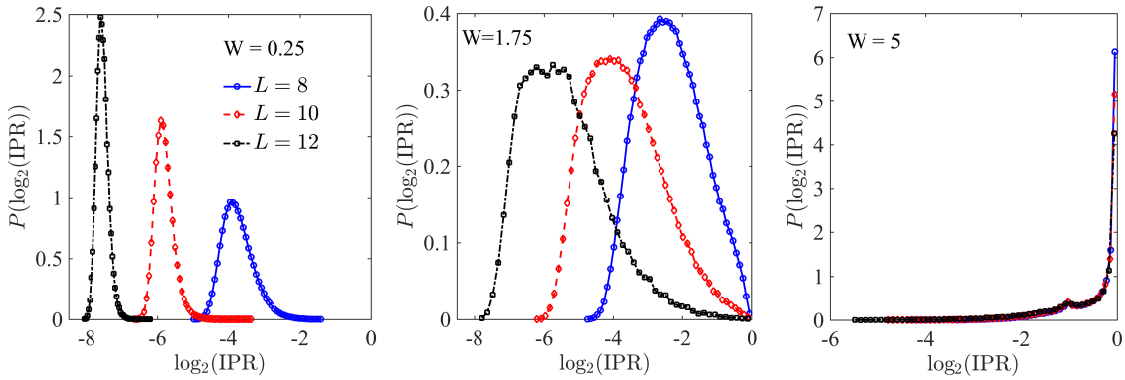

FIG. 3. (Color online) The distributions of $\log_2$ IPR in the middle of the band, $\epsilon \simeq 0.5$ for $W = 0.25$, 1.75 and 5 and the different number of spins $L = 8, 10$ and 12. The distributions are narrow in the ergodic and localized regimes, but are broader in the critical region $W = 1.75$.

states $|\psi\rangle$ that coincide with eigenstates $|\alpha_0\rangle$ of the initial Hamiltonian H_0 and have $S_z = 0$, where the state index $\alpha_0 = 1, \ldots N(L, 0)$ runs over eigenenergies of H_0 ordered in increasing order,

$$N(L, S) = \frac{L!}{(L/2 - S)!(L/2 + S)!}\,. \tag{5}$$

III. INVERSE PARTICIPATION RATIO

We demonstrate that the Hamiltonian $\tilde{H}$ with the quench still exhibits the MBL phase. As an indicator of MBL, we study the IPR defined as

$$\mathrm{IPR}_{\alpha_0} = \sum_{\tilde{\alpha}=1}^{2^L} |\langle\alpha_0|\tilde{\alpha}\rangle|^4 = \mathrm{Tr}\left\{\bar{\rho}_{\mathrm{DE}}^{|\alpha_0\rangle}\mathcal{P}_{\alpha_0}\right\}, \tag{6}$$

where $\mathcal{P}_{\alpha_0} = |\alpha_0\rangle\langle\alpha_0|$. The IPR is a measure of portion of the Hilbert space explored by the system after the perturbation V is turned on [19, 27, 29]. At weak disorder, the motion of the system is ergodic and the state spreads over a large fraction of the Hilbert space. As a result, the IPR is small $\sim 2^{-L}$. On the other hand, in the strong disorder limit, the ergodicity breaks down and the evolution of many-body wavefunctions is restricted to a small portion of the Hilbert space labeled by the local integral of motion [8]. This behavior of the IPR was recently discussed in connection of the survival probability near the MBL transition[30].

To investigate behavior of the IPR across the MBL transition we performed exact diagonalization for $L = \{8,\ 10,\ 12\}$ spins and $N = 2000$ realizations to obtain all eigenstates $|\alpha_0\rangle$ for H_0 and $|\tilde{\alpha}\rangle$ for $\tilde{H}$. We use these eigenstates to calculate the time average density matrix after a sudden quench $\rho_{\mathrm{DE}}^{|\alpha_0\rangle} = \sum_{\tilde{\alpha}} P_{\tilde{\alpha}}\,|\langle\tilde{\alpha}|\alpha_0\rangle|^2$ for a system that is initialized in eigenstate $|\alpha_0\rangle$ of H_0 with $S_z = 0$. The average $log_2(\mathrm{IPR})$ as a function of disorder strength W and ϵ is plotted in Fig. 2. Upon disorder average, $\log_2(\mathrm{IPR})(W, \epsilon)$ clearly reveals the existence of a mobility edge that distinguishes delocalized states to localized states; here $\epsilon = \alpha_0/N(L, 0)$ is the position of eigenstate within the energy band and the quench strength is fixed at $f = J = 1$ throughout our computations. To justify the nature of the mobility edge, we plot the histogram of the distribution of $\log_2$ IPR in Fig. 3. In the weak and strong disorder limit, the distributions of $\log_2$ IPR are highly concentrated at either $\propto (-L)$ or 0, respectively. However, $\log_2$ IPR in the crossover region is broadly distributed between $(-L)$ and 0 with its standard deviation $\propto L$ so that the standard deviation diverges at the mobility edge in the thermodynamic limit. We note that similar divergence has been found in the fluctuations of the entanglement entropy[17] and is due to similarity between entanglement entropy and IPR further investigated in [31].

When we fix the energy density at the middle of the band, $\epsilon \simeq 0.5$, the standard deviation of IPR has a peak in the crossover region at $W_c \simeq 3.5$, see Fig. 4(b). We note that at strong disorder, $W \simeq 5$, the standard deviation of IPR remain of the order of unity, indicating a broad distribution of the IPR in the localized regime. This behavior of the IPR in the middle of the energy band can be connected to the statistical orthogonality catastrophe [32]. Indeed, the overlap between the states before and after the quench varies significantly remaining close to unity for some states, while nearly vanishing for other states, see Ref. [33].

IV. LOCAL OBSERVABLES

A. Correlations for eigenstates

While the above approach to detect mobility edge through IPR is suitable for numerical calculations, it is hard to be realized experimentally because the eigenstates for a many-particle quantum system is almost im-

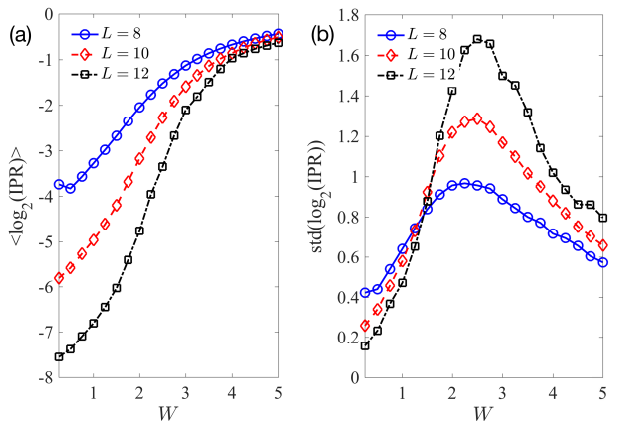

FIG. 4. (Color online) Average of the $\log_2(IPR)$ (a) and its standard deviation (b) over 1000 disorder realizations as functions of disorder strength W in the middle of the band, $\epsilon \simeq 0.5$ for a system of $L = 8, 10$ and 12 spins. The quench strength is fixed at $f = J = 1$.

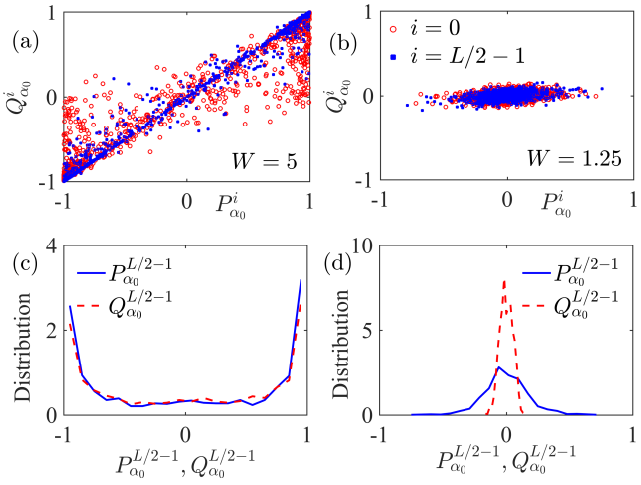

FIG. 5. (Color online) Scatter plot of $(P^i_{\alpha_0}, Q^i_{\alpha_0})$ for (a) the localized regime with $W = 5$ and (b) the ergodic regime with $W = 1.25$ for states $|\alpha_0\rangle$ in the middle of the band. Data obtained with $L = 12$ and $N = 1000$. Open circles (filled squares) show data for $i = 0$ ($i = L/2-1$). The corresponding probability distribution of P_i and Q_i are shown in panel (c) for the localized regime $W = 5$ and in panel (d) for the ergodic regime $W = 1.25$.

possible to prepare. Instead, we study the measurement of single spins in the time-averaged sense and investigate the correlation of their expectation values $\langle \sigma_z^{(i)} \rangle$ with and without a local perturbation. Our study is motivated by the previous observations[34] that in the MBL regime the ETH is violated and information about the local observables at sufficiently long times can be traced back to its initial condition resulting in correlations between spin states before and after perturbation V is turned on. Otherwise, in the delocalized regime the motion is ergodic and information about initial conditions is lost.

For an interacting system, the observables set by finite degrees of freedom can be evaluated by the reduced density matrices in which the off-diagonal elements are essentially zero due to dephasing even if the system starts in some arbitrary pure state. Alternatively, time averaged expectation values of a local operator are also characterized by a diagonal ensemble of the density matrix $\rho_{\rm DE}$, see Eq. (3). One can measure such local observables before and after the quench.

Here, we consider a special case of initial states that are eigenstates $|\alpha_0\rangle$ of H_0 and with $S_z = 0$, although the results remain qualitatively the same for a system that is initially prepared in an arbitrary pure state with $S_z = 0$, see below. We calculate expectation values $\langle \sigma_z^{(i)} \rangle$ of spin i before and after the quench at site 0:

$$P^i_{\alpha_0} = \langle \alpha_0 | \, \sigma_z^{(i)} \, | \alpha_0 \rangle \,, \tag{7a}$$

$$Q^i_{\alpha_0} = \sum_{\tilde\alpha} |\langle \alpha_0 | \tilde\alpha \rangle|^2 \, \langle \tilde\alpha | \, \sigma_z^{(i)} \, | \tilde\alpha \rangle = \mathrm{Tr} \left\{ \bar\rho_{\rm DE}^{|\alpha_0\rangle} \sigma_z^{(i)} \right\} . \tag{7b}$$

A good distinction between ergodic and MBL phases can be obtained by analyzing correlations between $P^i_{\alpha_0}$ and $Q^i_{\alpha_0}$. Running over all eigenstates $|\alpha_0\rangle$ in the $S_z = 0$ sector, we collect $P^i_{\alpha_0}$ and $Q^i_{\alpha_0}$ for a number of disorder realizations. In Fig. 5(a,b), we present the scatter plot for pairs of $(P^i_{\alpha_0}, Q^i_{\alpha_0})$ of spin $i = 0$ (directly perturbed spin, open circles) and $i = L/2 - 1$ (the farthest spin from the quench, filled squares) in the middle of the band, $\alpha_0 \simeq N(L, 0)/2$ for strong ($W = 5$) and weak ($W = 1.25$) disorder. In the localized phase at strong disorder, the local spin projection is good quantum number $P^i_{\alpha_0} \simeq \pm 1$ because eigenstates are product states consisting of physical spins $|\alpha\rangle = \bigotimes_i |\downarrow (\uparrow)\rangle_i$. Provided that the quench is smaller than the local random field, the eigenstates of H_0 and $\tilde H$ differ by terms $\mathcal{O}(f/W)$. As a consequence, the single spin measurement with and without a quench coincide with each other, see Fig. 5c for the distributions of $P^i_{\alpha_0}$ and $Q^i_{\alpha_0}$ peaked at ± 1. On the scatter plot, pairs $(P^{L/2-1}_{\alpha_0}, Q^{L/2-1}_{\alpha_0})$ are distributed along the line $P^{L/2-1}_{\alpha_0} = Q^{L/2-1}_{\alpha_0}$, indicating the two measurements are strongly correlated. In the ergodic phase at weak disorder ($W = 1.25$), an eigenstate is a linear combination of a large number of product states, and therefore local spin projection is not a good quantum number. Two sets of local spin measurements form an elliptic cloud in the center as a result of thermalization, see Fig. 5(b). Moreover, the distribution of single spin measurement shows disparity between the two cases due to the re-equilibration of the system after the perturbation, see Fig. 5(d).

Correlations between $P^i_{\alpha_0}$ and $Q^i_{\alpha_0}$ are characterized by the covariance with respect to disorder realizations:

$$C_{\alpha_0}(i) = \left\langle \delta P^i_{\alpha_0} \delta Q^i_{\alpha_0} \right\rangle_{H_0} , \tag{8}$$

where $\langle \dots \rangle_{H_0}$ stands for averaging over ensemble of H_0, $\delta P^i_{\alpha_0} = P^i_{\alpha_0} - \langle P^i_{\alpha_0} \rangle_{H_0}$ with the similar expression for

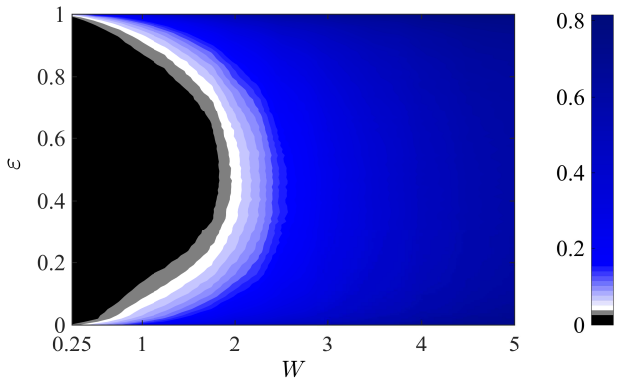

FIG. 6. (Color online) Covariance $C_{\alpha_0}(L/2-1)$ as functions of disorder strength W and energy density $\epsilon \propto \alpha_0$ for $L = 12$ and $N = 1000$. The crossover region to the MBL regime is shown in lighter colors.

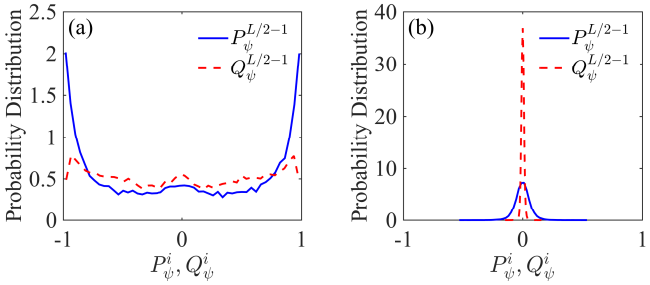

FIG. 7. (Color online) The probability distribution of P_i and Q_i for the localized regime with $W = 5$ (a) in which the single spin measurement with and without a quench coincides with each other and for the ergodic regime with $W = 1.25$ (b) the disparity in the distribution with and without the quench indicates a thermalization. Data obtained with $L = 12$ and $N = 1000$.

$\delta Q^i_{\alpha_0}$. We use the covariance to map out the phase diagram as a function W and $\epsilon = \alpha_0/N(L,0)$, as shown in Fig. 6. In the ergodic regime the averaged value $C_{\alpha_0}(L/2-1)$ vanishes but it saturates to 1 deep in the MBL phase where both $P^i_{\alpha_0}$ and $Q^i_{\alpha_0}$ take almost identical values $\sim (\pm 1)$. Similar to the IPR, $C_{\alpha_0}(i)$ reveals the many-body localization, marked by the border of the black region in Fig. (6).

B. Correlations for product states

Next, we analyze the correlations between a local operator before and after the quench for the case when an initial state is product state $|\psi\rangle = \bigotimes_i |\downarrow (\uparrow)\rangle_i$ with total $S_z = 0$. While signatures of the localization transition may be a bit blurry for such states, these states are more accessible in experiments. We again calculate the expectation values of $\langle \sigma_z^{(i)} \rangle$ of spin i for a system that undergoes long time evolution with respect to either H_0 or $\tilde{H}$:

$$P^i_\psi = \sum_{\alpha_0} \langle \alpha_0 | \sigma_z^{(i)} | \alpha_0 \rangle |\langle \psi | \alpha_0 \rangle|^2, \tag{9a}$$

$$Q^i_\psi = \sum_{\tilde{\alpha}} \langle \tilde{\alpha} | \sigma_z^{(i)} | \tilde{\alpha} \rangle |\langle \psi | \tilde{\alpha} \rangle|^2. \tag{9b}$$

At strong disorder, product states $|\psi\rangle$ are close to the eigenstates and only one term dominates in summations in Eqs. (9). In this sense, there is a well defined one-to-one mapping between product state $|\psi\rangle$ to the density matrix in the diagonal ensemble in such a way that there is a strong correlation between the two sets of measurement outcomes P^i_ψ and Q^i_ψ, see Fig. 7(a). Besides, the distribution of P_ψ at the farthest site $i = L/2-1$ is sharp at ± 1, while the distribution of Q_ψ at the same site is broadened due to the mixing between eigenstates arising from the perturbation term. In the opposite case when W is weak, a product state is a linear combination of a large number of eigenstates, indicating that in the mapping between diagonal ensemble and the initial product state is not invertible, see Fig. 7(b). Physically, as a prototype of ETH, this uninvertible mapping indicates that the system is thermalized regardless of its initial condition from the point of view of each eigenstate. The distribution of P^i_ψ and Q^i_ψ are both even sharper than the case shown in the previous subsection because the summation over all states $\tilde{\alpha}$ with different values S_z in Eq. (9) introduces additional averaging.

This behavior can be explained intuitively as follows. Eigenstates of H_0 in the ergodic regime are represented by a superposition of many products states, as one expects from analysis of IPR or other similar quantities. These products states will likely have the measured local spin in opposite directions. The projection of the local spin along z in an eigenstate direction averages over corresponding product state with non-zero overlap with the eigenstate. When the quench is turned on, the number of corresponding product states increases even more and the local spin projection reduces further. Notice that we have even narrow distribution when we look for P and Q evaluated for a product state. While at t=0, the spin projection is either ± 1, the time averaging is equivalent to taking a diagonal ensemble formed by many eigenstates. For each eigenstate we have a value $P^i_{\alpha_0}$, Eq. (7a) that varies between $\simeq (\pm 0.5)$ roughly symmetrically around zero. Performing additional averaging over eigenstates α_0 contributing to the diagonal density matrix results in reduced fluctuations of P^i_ψ, and after the quench is turned on, for Q^i_ψ.

V. LOCALIZATION LENGTH

With increasing spatial separation between the quenched spin and the monitored spin, we observe smaller deviations between $P^i_{\alpha_0}$ and $Q^i_{\alpha_0}$ as the effective coupling between the perturbed and monitored spins decreases fast as their separation exceeds the typical length of an eigenfunction. On the contrary, in the ergodic regime, the distribution of $(P^i_{\alpha_0},\ Q^i_{\alpha_0})$ is insensitive to the spatial separations between quench at site 0 and monitored spin i, suggesting that the eigenfuction extends throughout the whole system. The statistics of $P^i_{\alpha_0}$ and $Q^i_{\alpha_0}$ over ensemble of H_0 can be used to evaluate the localization length ξ. Intuitively, ξ is a scale below which a spin texture forms localized clusters and thereby the ergodicity is broken. Deep in the localized regime, localization occurs on atomic scales with $\xi \to 1$. With decreasing disorder, the localization length grows and once the scale is beyond the system size, the entire system cannot be decomposed into independent clusters and the ergodicity reoccurs. The localization length is an indicator of the onset of MBL regime that can be determined by the spatial sensitivity of the response to the local quench. The deviation between the measurement $P^i_{\alpha_0}$ and $Q^i_{\alpha_0}$ averaged over disorder realizations is given by "Euclidean distance":

$$D^i_{\alpha_0} = \sqrt{\left\langle (P^i_{\alpha_0} - Q^i_{\alpha_0})^2 \right\rangle_{H_0}}. \tag{10}$$

We argue that in the localized regime $D^i_{\alpha_0}$ is an exponentially decaying function[1, 15] with respect to the distance between spin i to the quenched spin:

$$D^i_{\alpha_0} \simeq D^0_{\alpha_0} \frac{\cosh((i - L/2)/\xi)}{\cosh(L/2\xi)} \tag{11}$$

where ξ is the localization length. The first two exponential terms in Eq. (11) arise from the periodic boundary condition, and the last term is a normalization constant. We plot $D^i_{\alpha_0}$ for spin $i = 0 \ldots 6$ obtained numerically for several different disorder strengths $W = 1.5, 2.5, 5$ for α_0 in the middle of the band and compare these data points to curves defined by Eq. (11) with the localization length evaluated as the best fit to data, see Fig. 8(a). In Fig. 8(b), we illustrate the fitted localization length ξ for different values of disorder W. Due to the finite size of the system, at the critical disorder $W_c \simeq 1.5$ the localization length ξ does not diverge but becomes larger than the system size, consistent with our argument about the crossover between ergodic and MBL phases. On the other hand, ξ saturates to unity at strong disorder in the MBL phase.

VI. LEVEL STATISTICS

We now discuss energy spectrum properties associated with a MBL Hamiltonian (1) subject to the quench (2).

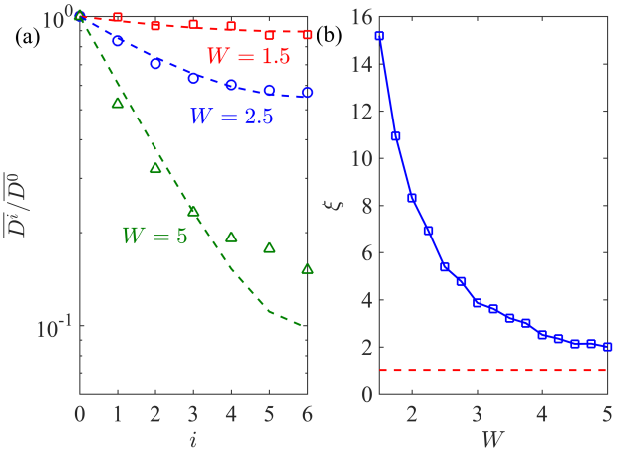

FIG. 8. (Color online) (a) "Euclidean distance" D^i as a function of distance between monitored spin and quenched spin (solid lines), and the corresponding fitting curve, Eq. (11) (dashed lines). (b) The many-body localization length ξ extracted from $D^{(i)}$ as a function of disorder strength. The dashed line corresponds to $\xi = 1$ to emphasize that the at sufficiently strong disorder W the system is localized at the atomic length scale.

The total spin projection $S_z = \sum_i \sigma_z^{(i)}$ is a conserved quantum number for H_0, while the quench term breaks the conservation of S_z. Quite generally, when the perturbation V is turned on, perturbed eigenstates contain corrections set by the matrix elements of the perturbation and by the differences in energies. As a consequence, energy levels acquire correlations.

The previous analysis of the level spacing statistics was focused on $S_z = 0$ subspace[2]. Here we consider full energy level statistics that include all eigenvalues of global S_z when neighboring levels may belong to different values of S_z and remain completely independent for the Hamiltonian (1). Consequently, the full level spacing statistics will be close to the Poissonian in the absence of quench.

To characterize the mixing of eigenstates from different eigenvectors of S_z, we examine the distribution of the difference in indexes $\Delta\alpha_0$ for states in the $S_z = 0$ sector. Fig. 9 shows the distribution of $\Delta\alpha_0$ for both ergodic and localized regimes. In both regimes, the probability to have two states with $S_z = 0$ next to each other is relatively small: in the localized regime, only $\simeq 23\%$ of states have neighbor from $S_z = 0$ sector, this fraction is even lower, $\simeq 9\%$, for the ergodic regime. In other words, in ergodic regime, two adjacent eigenvalues are much more likely from two different families of S_z, rather than from the same value. Reduction of the fraction of neighbors with $S_z = 0$ in the ergodic regime reflects the rigidity of energy spectrum of unperturbed H_0: eigenstates with $S_z = 0$ appear with more regular spacings due to the level repulsion. In this case, eigenstates of H_0 with $S_z \neq 0$ fill in between the eigenstates with $S_z = 0$ and reduce frac-

tion of states with $\Delta\alpha_0 = 1$ or 2, see Fig. 9.

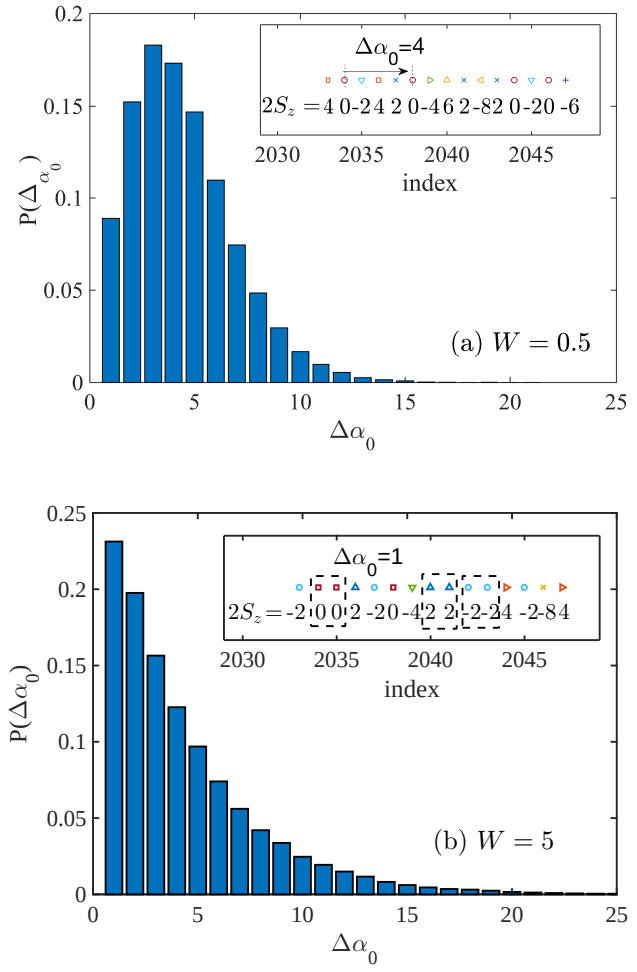

FIG. 9. (Color online) The distribution of $\Delta\alpha_0$ for the $S_z = 0$ sector of the spectrum in (a) the ergodic regime, $W = 0.5$, or (b) the localized regime, $W = 5$. Data is obtained for $L = 12$ with 100 disorder realizations. Insets: the pattern of states labeled by different S_z in the middle of the band for one arbitrary disorder realization. Different markers correspond to different S_z. In the ergodic regime, states with the same S_z are more likely separated by at least one state with a different S_z, whereas for the localized regime, states with the same S_z more likely appear in adjacent pairs.

Next, we consider the distribution function $P(r)$ of the dimensionless parameter[2, 35]

$$r_n = \frac{\min(\delta_n, \delta_{n+1})}{\max(\delta_n, \delta_{n+1})}, \tag{12}$$

where δ_n is the energy separation between adjacent many-body eigenstates $\delta_n = E_{n+1} - E_n$. This parameter is dimensionless and independent of local density of states. Thus such a distribution permits a transparent distinction from the band edges to the dense part of the spectrum.

As shown in Refs. [2] in the localized regime, the eigenenergies for S_z=0 are uncorrelated and therefore the probability distribution of δ_n is Poisson, which corresponds to $P_P(r) = 2/(1+r)^2$. On the other hand, in the ergodic regime, the level spacing is phenomenologically described by the random matrix theory, where the eigenvalues are correlated due to level repulsion. In this case one expects the Wigner-Dyson statistics of eigenenergies and $P(r) \to 0$ at small r [35].

When the entire spectrum representing all values of S_z is considered without the quench, the distribution of $P(r)$ is very close to that of the Poisson distribution $P_P(r)$, see Fig. 10. Indeed, as we discussed above, both in the ergodic and localized regimes, the nearest energy states most likely belong to different eigenvalues of S_z and are uncorrelated for H_0 without a quench. The situation changes when the quench is turned on. The full quantum energy statistics unveil its localized or ergodic behavior. To demonstrate this, we vary the amplitude of the drive from f for each disorder realization keeping other parameters of the model fixed for both ergodic and localized regimes. For each realization of H_0, we compute values of r for the entire spectrum and build histograms $P(r)$ for distribution of parameter r. In Fig. 10, we present $P(r)$ for $W = 0.5$ and $W = 5$. For strong disorder, $W = 5$, even though the perturbation induce a finite matrix element between states with different S_z, this effect on level spacing statistics is minor because a considerable portion of eigenstates are still being localized and remain uncorrelated. Consequently from the distribution function $P(r)$ for finite drive amplitude at small r there is no apparent level repulsion. On the other hand for weak disorder, $W = 0.5$, the spectrum is sensitive to the quench as its matrix elements do not vanish between different eigenstates of H_0. As f grows, signature of level repulsion quickly reveals at $f \gtrsim 0.1J$, as shown in Fig. 10.

The onset of level repulsion can be quantified by looking at the "maximum distance" (MD) between cumulative distributions r, $Q_\alpha(r) = \int_0^r P_\alpha(r')dr'$ between the Poisson, $P_P(r)$, and actual, $P_a(r)$, distributions:

$$\text{MD} = \left| \int_0^{r_0} (P_P(r) - P_a(r))\, dr \right|, \tag{13}$$

where $P_p(r) = 2/(1+r)^2$ is the Poisson distribution function for r and the limit of integration r_0 is chosen to maximize the difference in the cumulative distributions $|Q_a(r) - Q_P(r)|$, i.e., the first intersection point of $P_P(r)$ and $P_a(r)$. The advantage of this functional distance of the distribution functions $P_P(r)$ and $P_a(r)$ is that the data of cumulative distribution $Q(r)$ is less noisy than $P(r)$ itself and captures well the onset of level repulsion which drastically changes statistics of small values of r.

The dependence of MD on amplitude of drive has different behavior in the two phases, as shown in Fig. 11. In our numerics, the cumulative distribution of $Q(r)$ is obtained by the labels of sorted data of r. In this manner, even for 100 disorder realizations, $Q(r)$ is smooth enough for computation purposes. In the ergodic regime, the MD

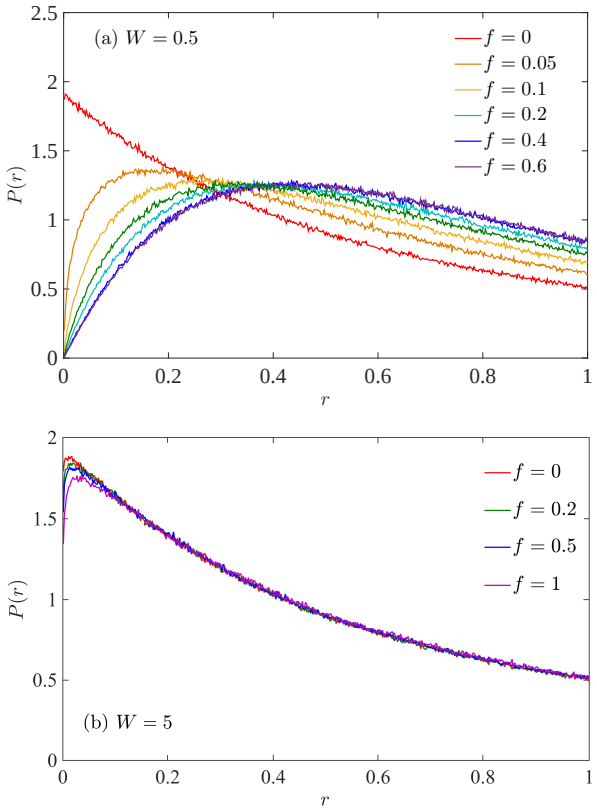

FIG. 10. (Color online) The probability distribution of r for (a) the ergodic regime, $W = 0.5$ and (b) the localized regime, $W = 5$ with varying amplitude of perturbation f. Data is obtained for $L = 12$ with 1000 disorder realizations.

quickly saturates to $\simeq 0.24$ at $f \simeq 0.4J$, while in the localized regime the MD remains constant at a small value $\simeq 0.01$.

It is worth pointing out that our numerical result for the distribution of r for the entire spectrum agrees with the previous studies of the average of r for $S_z = 0$ subspace. Namely, $\langle r \rangle \simeq 0.39$ for Poisson distribution and $\langle r \rangle \simeq 0.53$ for GOE. However, we prefer to use the MD instead of $\langle r \rangle$ as a measure to distinguish the distributions is that the MD better distinguishes behavior of $P(r)$ at small values of r rather than by the whole range $0 < r < 1$.

VII. SUMMARY AND CONCLUSIONS

To summarize, we showed that as a result of local quench, the absence of thermalization in the MBL phase can be characterized by the IPR of the eigenstates of the original Hamiltonian in the basis of the quenched Hamiltonian. In particular, the IPR fluctuations are enhanced at the crossover between the ergodic and MBL phases. Meanwhile, our analysis of the single spin measurements in response to a quench shows a plausible experimental

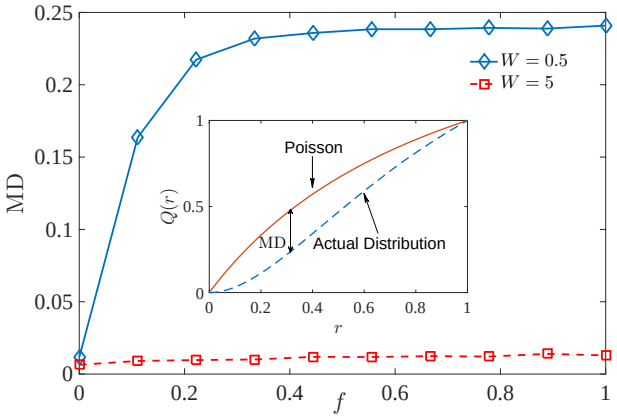

FIG. 11. (Color online) Dependence of MD on the amplitude of perturbation f for weak ($W = 0.5$) and strong ($W = 5$) disorder. As a measure of deviation from Poisson statistics, the MD for the ergodic regime is sensitive on f and grows quickly to $\simeq 0.24$, while for the localized regime MD roughly remains constant at a small value $\simeq 0.01$. Inset: The definition of MD is given by the maximum distance between cumulative distribution functions of r between Poisson statistics and actual statistics.

technique to search for the mobility edge and the localization length. This approach does not require substantial measurements of a quantum system as compared to more complicated measurement of many-particle entanglement. Our analysis demonstrated that for a system with MBL behavior, simple single spin measurement can reveal the indispensable characteristics, complementary to more sophisticated routes to check the growth of entanglement entropy[12, 13] or quantum revivals[36] under time resolution.

The local transverse field couples states with different total spin S_z along z direction and extends the Hilbert space of the original system with $S_z = 0$ and dimension N(L,S), Eq. (5) to the entire 2^L dimensional space of L spins. We also demonstrated that a local transverse field directly probes the appearance of level repulsion in the delocalized phase, while level spacing statistics remain Poisson in the MBL phase with a transverse quench. In the delocalized regime at weak disorder, this quench effectively leads to thermolization of the system in in this extended Hilbert space, while in the MBL regime such thermolization does not occur.

Acknowledgements.– We thank D. Basko, D. Huse, L. Ioffe, R. Nandkishore, V. Oganesyan and P. Woelfle for fruitful discussions. This work is supported by NSF Grant No. DMR-0955500.

[1] D. M. Basko, I. L. Aleiner, and B. L. Altshuler, Ann. Phys. (N. Y). **321**, 1126 (2006), 0506617.

[2] V. Oganesyan and D. A. Huse, Phys. Rev. B **75**, 155111 (2007).

[3] I. V. Gornyi, A. D. Mirlin, and D. G. Polyakov, Phys. Rev. Lett. **95**, 206603 (2005).

[4] M. Schreiber, S. S. Hodgman, P. Bordia, H. P. Lüschen, M. H. Fischer, R. Vosk, E. Altman, U. Schneider, and I. Bloch (2015), 1501.05661.

[5] C. Senko, J. Smith, P. Richerme, A. Lee, W. C. Campbell, and C. Monroe, Science (80-.). **345**, 430 (2014).

[6] R. Islam, C. Senko, W. C. Campbell, S. Korenblit, J. Smith, A. Lee, E. E. Edwards, C.-C. J. Wang, J. K. Freericks, and C. Monroe, Science (80-.). **340**, 583 (2013).

[7] R. Barends, L. Lamata, J. Kelly, L. García-Álvarez, A. G. Fowler, A. Megrant, E. Jeffrey, T. C. White, D. Sank, J. Y. Mutus, et al., Nat. Commun. **6**, 7654 (2015), 1501.07703.

[8] M. Serbyn, Z. Papić, and D. A. Abanin, Phys. Rev. Lett. **111**, 127201 (2013).

[9] A. Chandran, I. H. Kim, G. Vidal, and D. A. Abanin, Phys. Rev. B **91**, 085425 (2015).

[10] V. Ros, M. Müller, and A. Scardicchio, Nucl. Phys. B **891**, 420 (2015).

[11] I. H. Kim, A. Chandran, and D. A. Abanin (2014), 1412.3073.

[12] J. H. Bardarson, F. Pollmann, and J. E. Moore, Phys. Rev. Lett. **109**, 017202 (2012).

[13] M. Serbyn, Z. Papić, and D. a. Abanin, Phys. Rev. Lett. **110**, 260601 (2013), 1304.4605.

[14] A. Nanduri, H. Kim, and D. A. Huse, Phys. Rev. B **90**, 064201 (2014).

[15] M. Serbyn, Z. Papić, and D. A. Abanin, Phys. Rev. B **90**, 174302 (2014).

[16] R. Vosk and E. Altman, Phys. Rev. Lett. **112**, 217204 (2014).

[17] J. A. Kjäll, J. H. Bardarson, and F. Pollmann, Phys. Rev. Lett. **113**, 107204 (2014).

[18] W. de Roeck, F. Huveneers, M. Müller, and M. Schiulaz, p. 5 (2015), 1506.01505.

[19] S. Bera, H. Schomerus, F. Heidrich-Meisner, and J. H. Bardarson, Phys. Rev. Lett. **115**, 046603 (2015), 1503.06147.

[20] M. Serbyn, Z. Papić, and D. A. Abanin, Phys. Rev. X **5**, 041047 (2015), 1507.01635.

[21] K. Agarwal, S. Gopalakrishnan, M. Knap, M. Müller, and E. Demler, Phys. Rev. Lett. **114**, 1 (2015), 1408.3413.

[22] S. Gopalakrishnan, M. Müller, V. Khemani, M. Knap, E. Demler, and D. A. Huse, Phys. Rev. B - Condens. Matter Mater. Phys. **92**, 1 (2015), 1502.07712.

[23] D. J. Luitz, N. Laflorencie, and F. Alet, Phys. Rev. B **91**, 081103 (2015), 1411.0660.

[24] I. Mondragon-Shem, A. Pal, T. L. Hughes, and C. R. Laumann, p. 10 (2015), 1501.03824.

[25] A. Pal and D. A. Huse, Phys. Rev. B **82**, 174411 (2010).

[26] R. Vosk, D. Huse, and E. Altman, arXiv Prepr. arXiv1412.3117 pp. 1–13 (2014), 1412.3117.

[27] D. M. Basko, I. L. Aleiner, and B. L. Altshuler, *Problems of Condensed Matter Physics: Quantum coherence phenomena in electron-hole and coupled matter-light systems.* (Oxford University Press, 2007), ISBN 9780199238873, 0602510.

[28] M. Rigol, V. Dunjko, and M. Olshanii, Nature **452**, 854 (2008).

[29] A. De Luca and A. Scardicchio, EPL (Europhysics Lett. **101**, 37003 (2013).

[30] E. J. Torres-Herrera and L. F. Santos, Phys. Rev. B **92**, 014208 (2015), 1501.05662.

[31] W. Beugeling, A. Andreanov, and M. Haque, J. Stat. Mech. Theory Exp. **2015**, P02002 (2015), 1410.7702.

[32] V. Khemani, R. Nandkishore, and S. L. Sondhi, Nat. Phys. **11** (2015).

[33] D.-L. Deng, J. H. Pixley, X. Li, and S. D. Sarma, pp. 1–8 (2015), 1508.01270.

[34] R. Nandkishore and D. A. Huse, Annu. Rev. Condens. Matter Phys. **6**, 15 (2015).

[35] Y. Y. Atas, E. Bogomolny, O. Giraud, and G. Roux, Phys. Rev. Lett. **110**, 084101 (2013), 1212.5611.

[36] R. Vasseur, S. A. Parameswaran, and J. E. Moore, Phys. Rev. B **91**, 140202 (2015).